Direct Ab Initio Dynamics Study of Radical C4H ((X)over-tilde(2)Sigma(+)) + CH4 Reaction

ARTICLE *in* THE JOURNAL OF PHYSICAL CHEMISTRY A · MARCH 2011

Impact Factor: 2.69 · DOI: 10.1021/jp200231n · Source: PubMed

5 AUTHORS, INCLUDING:

Xiang Zhang
Shanxi Teachers University
21 PUBLICATIONS **194** CITATIONS
SEE PROFILE

Dan Mu
Jilin University
166 PUBLICATIONS **1,135** CITATIONS
SEE PROFILE

Jilai Li
Jilin University
66 PUBLICATIONS **287** CITATIONS
SEE PROFILE

THE JOURNAL OF PHYSICAL CHEMISTRY A

ARTICLE

pubs.acs.org/JPCA

Direct Ab Initio Dynamics Study of Radical C_4H ($\tilde{X}^2\Sigma^+$) + CH_4 Reaction

Rui-Ping Huo,[†] Xiang Zhang,[‡] Xu-Ri Huang,[†] Ji-Lai Li,[*,†] and Chia-Chung Sun[†]

[†]State Key Lab of Theoretical and Computational Chemistry, Institute of Theoretical Chemistry, Jilin University, Changchun 130023, People's Republic of China

[‡]School of Chemistry and Materials Science, Shanxi Normal University, Linfen 041004, People's Republic of China

Supporting Information

ABSTRACT: The methane (CH_4) hydrogen abstraction reaction by linear butadiynyl radical C_4H (CCCCH) has been investigated by direct ab initio dynamics over a wide temperature range of 100−3000 K, theoretically. The potential energy surfaces (PESs) have been constructed at the CCSD(T)/aug-cc-pVTZ//BB1K/6-311G(d,p) levels of theory. Two different hydrogen abstraction channels by C^1 and C^4 of C_4H ($C^1C^2C^3C^4H$) have been considered. The results indicate that the C^1 position of C_4H is a more reactive site. The electron transfer behaviors of two possible channels are also analyzed by quasi-restricted orbital (QRO) in detail. The rate constants calculated by canonical variational transition-state theory (CVT) with the small-curvature tunneling correction (SCT) are in excellent agreement with available experimental values. The normal and three-parameter expressions of Arrhenius rate constants are also provided within 100−3000 K. It is expected to be helpful for further studies on the reaction dynamics behaviors over a wide temperature range where no experimental data is available so far.

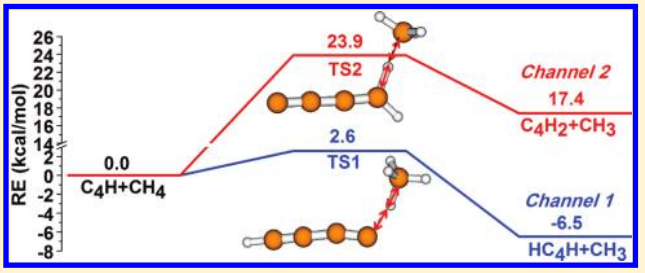

1. INTRODUCTION

Hydrogen-deficient molecules C_nH are important intermediates in combustion flames,[1−3] planetary atmospheres,[4,5] and astrochemistry.[6] Among free hydrocarbon radicals, the linear butadiynyl C_4H molecule is a key member of the C_nH series of molecules that has received particular attention due to its potential importance as a precursor to polycyclic aromatic hydrocarbons (PAHs) and possibly to fullerenes[7] in interstellar medium,[8−10] in combustion processes,[1−3] and in hydrocarbon-rich atmospheres of planets and their moons.[4,5] The discovery of C_4H was in one of the first electron spin resonance (ESR) spectroscopic identifications of long carbon chain free radicals containing four or more atoms in the gas phase.[11] And then laboratory experiments were performed in the gas phase and in rare gas matrices.[12−16] The C_4H radical has also been detected in many important astronomical sources. The first observation was in low-temperature argon and neon matrices in its electronic ground state,[11] in the dark molecular cloud TMC-1.[17−20] It was observed again in the circumstellar envelope of the dying carbon star IRC+10216[21] by radioastronomy and subsequently in the taurus molecular cloud.[22] In interstellar molecular clouds (IMCs), the butadiynyl radicals are surprisingly more abundant than many common molecules, such as CH_3CHO, CH_3OH, HCOOH, CH_3CN, C_3H_2, C_4H_2, and HC_3N.[9,10,16]

These investigations stimulated extensive theoretical work, such as structural optimizations and excited state calculations using Hartree−Fock calculations[23,24] and correlated methods.[14−25] Previous studies demonstrated there are two low-lying states, $\tilde{X}^2\Sigma^+$ and $\tilde{A}^2\Pi$ symmetry. The $\tilde{X}^2\Sigma^+$ state has a much smaller dipole moment than the $\tilde{A}^2\Pi$ one. The energy difference between the couple states of C_4H is very sensitive to the methods chosen. The accurate values for the energetic separation between $\tilde{X}^2\Sigma^+$ and $\tilde{A}^2\Pi$ states of the radical C_4H and C_4D have also been established.[26] Most studies[1,14,25] found that the $\tilde{X}^2\Sigma^+$ state is the ground state and the $\tilde{A}^2\Pi$ is the lowest-lying excited one, in agreement with experimental findings.[11,14]

The kinetics study of the reactions of C_4H radical $\tilde{X}^2\Sigma^+$ state with various hydrocarbons among the most abundant observed in Titan's atmosphere (CH_4, C_2H_2, C_2H_4, C_2H_6, CH_3C_2H, and C_3H_8) have been studied directly.[27] However, published experimental data is still rather limited hereto. The experimental rate constants of the reaction $C_4H + CH_4$ are available only at 200 K (7.70×10^{-13} cm^3 $molecule^{-1}$ s^{-1}) and 300 K (2.13×10^{-12} cm^3 $molecule^{-1}$ s^{-1}), respectively.[27] Picard and co-workers[27] proposed that the rate constants of C_4H with hydrocarbons should be negative temperature-dependent, except for the reaction with methane. To the best of our knowledge, the relevant data available in a wide temperature regime remains incomplete and there is no available theoretical study of this reaction despite its particular importance. With this stimulus, we therefore performed direct ab initio dynamics study on the title reaction C_4H ($\tilde{X}^2\Sigma^+$) + CH_4. Our aims are to investigate the possible reaction mechanisms and feasible channels, to obtain "accurate" theoretical rate constants and to explore to what

Received: January 9, 2011
Revised: March 7, 2011
Published: March 28, 2011

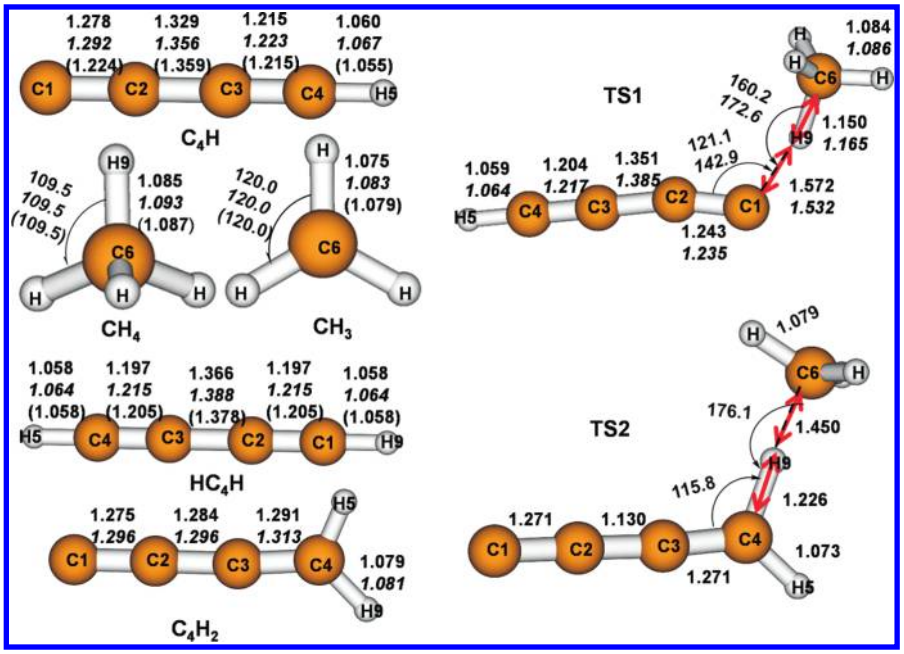

Figure 1. Geometric parameters of various species involved in the title reaction. Bond length in angstrom and angle in degree. The normal, italics, and in parentheses are at the BB1K/6-311G(d,p), UCCSD/6-31G(d,p) levels, and experimental data, respectively. The red arrows show the harmonic vibrational mode in the transition state. Experimental data: CH_4, refs 41 and 42; C_4H, ref 14; CH_3, ref 43; HC_4H, ref 44.

extent the theory predictions could be compared with available experimental results over the temperature range 200−300 K.[27] The temperature dependence of the rate constants is also provided in this study over a wide temperature region of 100−3000 K for future study.

2. COMPUTATIONAL METHODS

The geometries of the reactants, products, intermediates, and transition states (TSs) involved in the title reaction were fully optimized at the BB1K/6-311G(d,p) level of theory.[28] The minimum energy pathway (MEP) was obtained by intrinsic coordinate (IRC) theory, with a gradient step-size of 0.05 $(amu)^{1/2}$ bohr. Then, the first and second energy derivatives were obtained to calculate the curvature of the reaction path and the generalized vibrational frequencies along the reaction pathways. To obtain more accurate energies and barrier height, the single point energies (SPE) were refined by the coupled-cluster (CC) theory[29] of triple excitations CCSD(T) method[30] with 6-311G(2df,p) (B2), 6-311++G(3df,2pd) (B3), and aug-cc-pVTZ (B4) basis sets using the BB1K-optimaized geometries, respectively. It should be noted here that we also performed geometric optimization at the CCSD/6-31G(d,p) levels to verify the BB1K structural parameters. All the electronic structural calculations were performed by Gaussian03 program package.[31]

By means of the POLYRATE 9.7 program package,[32] the theoretical rate constants and activation energies were calculated using the conventional transition state theory (TST),[33] canonical variational transition-state theory (CVT),[34,35] and canonical variational transition state incorporating a small-curvature tunneling correction (CVT/SCT) method.[33] The Euler single-step integrator with a step size of 0.001 $(amu)^{1/2}$ bohr was used to follow the MEP. The curvature components were calculated using a quadratic fit to obtain the derivative of the gradient with respect to the reaction coordinate. Within the temperature range 100−3000 K, the rate constants at various temperature points were calculated using mass-scaled Cartesian coordinate.

Quasi-restricted molecular orbital (QRO)[36] of selected points along the MEP were calculated by ORCA 2.8 program package[37] and plotted using Chimera.[38]

3. RESULTS AND DISCUSSION

3.1. Stationary Points. Depending on the position of C_4H that CH_4 attacks, two distinguishable channels are considered as follows:

Channel 1: hydrogen abstraction by C^1 of C_4H

$$\bullet{}^1C \equiv C^2 - C^3 \equiv C^4H + CH_4 \rightarrow H^1C \equiv C^2 - C^3 \equiv C^4H + \bullet CH_3 \quad (a)$$

Channel 2: hydrogen abstraction by C^4 of C_4H

$$\bullet{}^1C \equiv C^2 - C^3 \equiv C^4H + CH_4 \rightarrow {}^1C \equiv C^2 - C^3 = C^4H_2 + \bullet CH_3 \quad (b)$$

The geometric parameters of the reactants, products, and transition states of the two channels optimized at the BB1K/6-311G(d,p) and CCSD/6-31G(d,p) levels are shown in Figure 1. Available experimental values are also given. The coordinates and harmonic frequencies of the reactants, products, and transition states and available experimental values are listed in Supporting Information in Tables S1−S4. In Figure 1, selected bond lengths and angles are given. The geometry parameters of all species calculated by both BB1K and CCSD methods can predict rational geometrical parameters, and the discrepancies are negligible compared with experimental data.

As shown in Figure 1, one can find that in the transition structure TS1 involved in Channel 1, the length of bond C6−H9 to be broken increases by 6% compared with the equilibrium bond length of C−H in CH_4. The length of C1−H9 bond to be

dx.doi.org/10.1021/jp200231n |J. Phys. Chem. A 2011, 115, 3576–3582

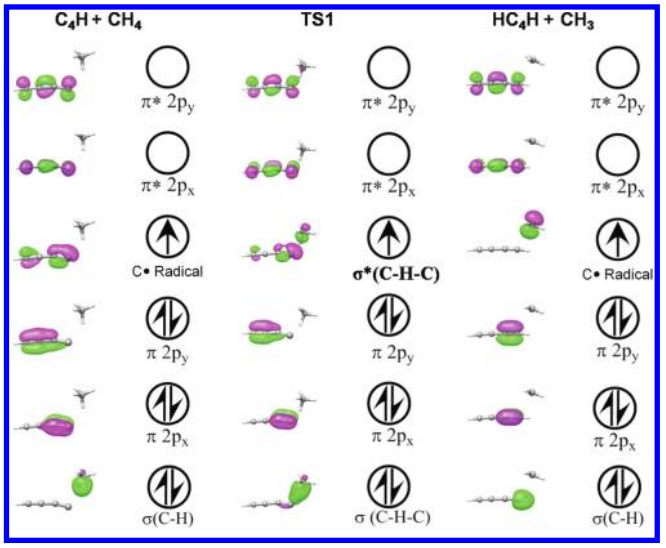

Figure 2. Schematic MO diagrams of reactants ($C_4H + CH_4$), transition state (TS1), and products ($HC_4H + CH_3$).

formed is 1.5 times as the equilibrium bond length of C1−H9 in H−C_4−H. Hence, the less stretch of the breaking bond than that of the forming bond indicates a reactant-like transition state TS1, that is, the H-abstraction channel process is via an early transition state. The harmonic vibrational frequencies of all the reactants and products at the BB1K/6-311G(d,p) level are also in good agreement with available experimental data.[6,39,40] The TS1 possesses one and only one imaginary frequency −342 cm^{-1}, indicating that the transition state is a real first-order saddle point. While for the TS2 in Channel 2 (Figure 1), the length of C6−H9 bond to be broken is stretched by 34% over that in reactant CH_4 and the C4−H9 bond to be formed is about 14% longer than that in product C_4H_2. Hence, the more stretch of the breaking bond than that of the forming bond indicates a product-like transition state TS2, namely, the H-abstraction channel process is via a late transition state.

3.2. Electron Transfer Behaviors. The detailed electron transfer analysis is carried out along the minimal energy pathway by quasi-restricted molecular orbital calculations using ORCA program. Figure 2 and Figure S1 present the schematic frontier molecular orbital (FMO) diagrams for the reactants, transition states, and products involved in Channels 1 and 2, respectively. As shown in Figure 2, we can see that as the C_4H and CH_4 approaches to each other, the delocalized π bond formed among C2, C3, and C4 atoms in reactant is gradually shifted to C2 and C3 atoms, leading to the radical character mainly localized on C1. At the same time, the elongated C−H bond in CH_4 is weakened. In agreement with the geometric structure analysis discussed above that indicates an early transition state, the electronic structure of TS1 only involves weak interactions between $\sigma_{(C-H)}$ in CH_4 and $C^\bullet$ radical orbital of C_4H, which is evidenced by less significant electron transfer during this process. From TS1 to product, it becomes evident that one β electron in C−H bond of CH_4 is shifted to the π_{2p}-orbital ($\sigma^*_{(C-H-C)}$) of C_4H, leading to the CH_3 moiety with one α electron left. By analysis of the corresponding molecular orbital, we can draw the conclusion that this reaction pathway proceeds through the classical hydrogen-atom transfer (HAT) mechanism. Schematically as shown in Figure 2, one proton and electron in the C−H bond of CH_4 are transferred concomitantly to the singly occupied orbital on $C^\bullet$ radical in C_4H.

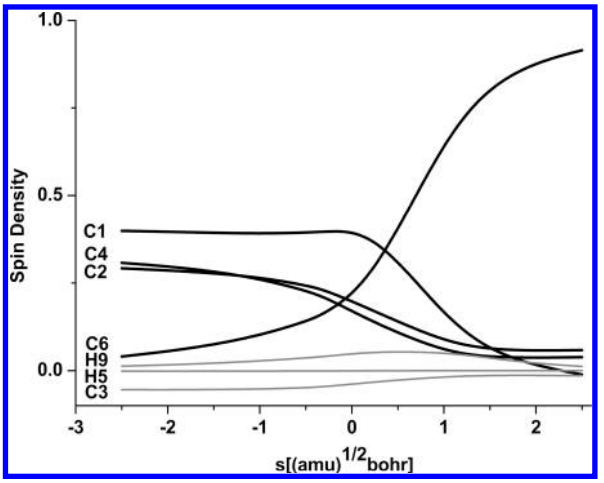

Figure 3. The change of atomic spin densities on C1, C2, C3, C4, H5, C6, and H9 obtained from selected points on IRC pathway by ORCA program.

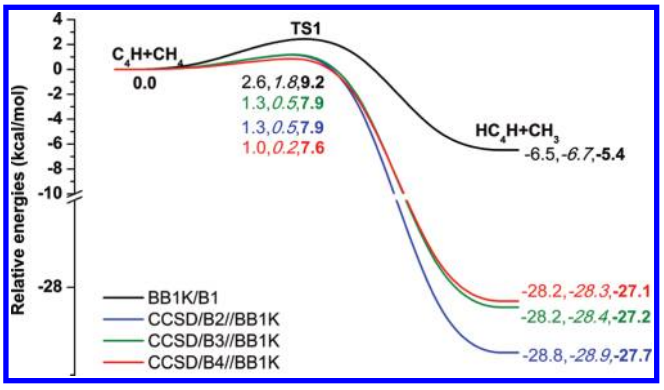

Figure 4. Potential energy profiles for the reaction of C_4H ($\tilde{X}^2\Sigma^+$) + $CH_4 \rightarrow CH_3 + HC_4H$. Black line, BB1K/B1; blue line, CCSD(T)/B2//BB1K/B1; green line, CCSD(T)/B3//BB1K/B1; red line, CCSD(T)/B4//BB1K/B1. The normal, italics, and bold values are ΔE, ΔH, and ΔG, respectively (unit: kcal/mol).

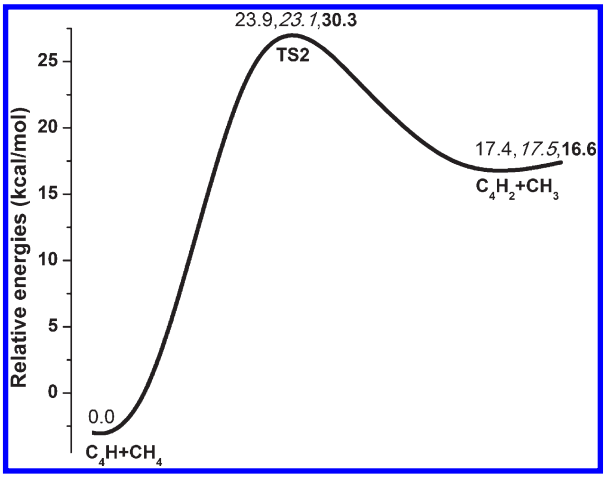

Figure 5. Potential energy profiles at the BB1K/B1 level for the channel 2 of the reaction C_4H ($\tilde{X}^2\Sigma^+$) + $CH_4 \rightarrow CH_3 + C_4H_2$. The normal, italics, and bold values are ΔE, ΔH, and ΔG, respectively (units: kcal/mol).

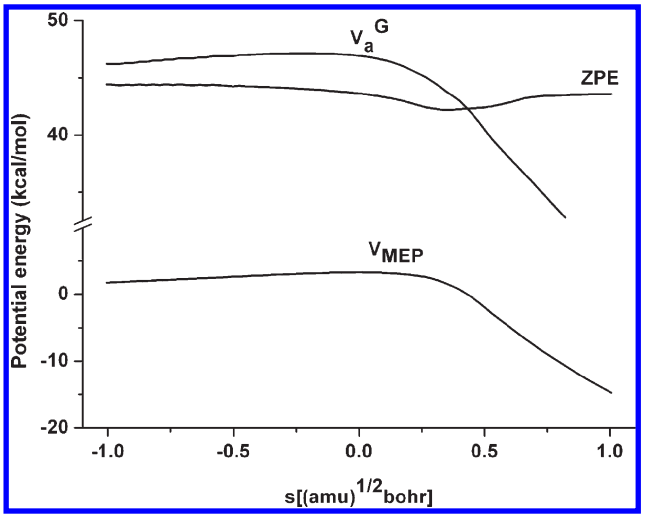

Figure 6. Classical potential energy curve (V_{MEP}), ground-state vibrationally adiabatic curve (V_a^G), and ZPE curve as functions of s [(amu)$^{1/2}$ bohr] at the CCSD(T)/B4//BB1K/B1 levels for the title reaction.

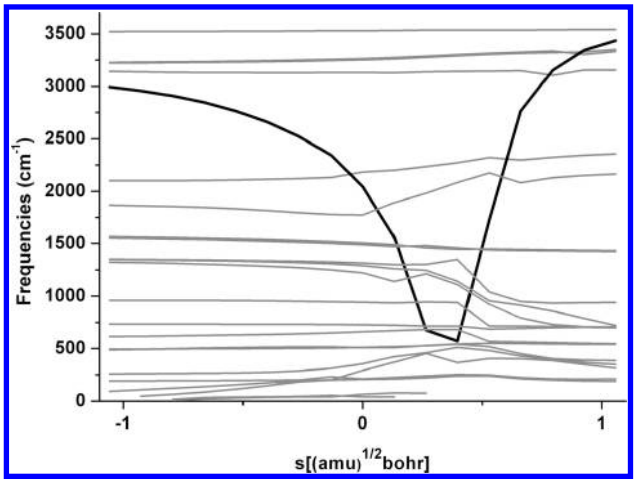

Figure 7. Changes of the generalized normal mode vibrational frequencies along the MEP as functions of intrinsic reaction coordinate s at the BB1K/6-311G(d,p) level.

Figure 3 gives the spin density changes upon the reaction process of Channel 1. As the reaction going on, the spin density of C6 increased concomitantly with that decreased in C1, C2, and C4. Moreover, the spin densities of H9, H5, and C3 are nearly unchanged. To sum up, the overall mechanism of the title reaction can be better described as following: as CH_4 and C_4H gradually approach with each other, one of H-atoms in CH_4 is abstracted by one C^1 atoms in C_4H, leading to H−C_4−H and one radical $^{\bullet}CH_3$ generation.

3.3. Energetics. As shown in Figures 4 and 5, our calculated barrier heights with zero-point energy (ZPE) correction at the BB1K/6-311G(d,p) level are to be 2.6 and 23.9 kcal/mol for Channels 1 and 2, respectively. Due to lower barrier height of Channel 1, it is obvious that this channel should be considered as a dominant pathway. To construct a reliable MEP for the rate constant calculations, we further refined the single point energies (SPE) of stationary points using CCSD(T) method with basis sets B2, B3, and B4, respectively. The electronic structural energies, zero-point correction energies and relative energies of all stationary points at various levels of theory are listed in Tables S5−S8.

The barriers and reaction energies of the Channel 1 obtained at the BB1K/B1, CCSD(T)/B2//BB1K, CCSD(T)/B3//BB1K, and CCSD(T)/B4//BB1K levels in the present study are given in Figure 4. The total energy of the reactants C_4H + CH_4 is set to zero as a reference for other species involved in the title reaction. As shown in Figure 4, among the four levels of theory, the energy barrier heights ΔE decrease (2.6 → 1.3 → 1.3 → 1.0 kcal/mol) along with the increasing of basis sets B1 → B2 → B3 → B4, and the CCSD(T)/B4 gives the lowest effective energy barrier 1.0 kcal/mol. This tendency suggests that, given larger basis sets used, the barrier height is very likely to become close to that of experimental value.[27] The barrier height of CCSD(T)/B4 seems to be more reliable. The reaction enthalpies (ΔH_{298}^{Φ}) of the C_4H + CH_4 reactions are listed in Table S8. The BB1K and CCSD(T) methods estimate Channel 1 exothermic by −6.7, −28.9, −28.4, and −28.3 kcal/mol for BB1K/B1, CCSD(T)/B2//BB1K, CCSD(T)/B3//BB1K, and CCSD(T)/B4//BB1K, respectively. Clearly, the CCSD(T)/B4 result is in better agreement with the experimental values (−28.2 kcal/mol).[27] Considering the efficiency and precision, it is therefore safe to make the conclusion that the combination of the CCSD(T)/B4//BB1K/B1 methods can provide satisfied results for analogous systems. So, we refined the SPE of selected points on the BB1K MEP using the CCSD(T)/B4 method for the following rate constant calculations.

3.4. Dynamics Calculations. The MEP for Channel 1 is calculated by IRC at the BB1K/6-311G(d,p) level (energies, gradients, and Hessians). Figure 6 depicts the plot of the classical potential energy curve $V_{MEP(s)}$, the vibrationally adiabatic ground-state potential curve $V_{a\,(s)}^G$, and the zero-point energy profile (ZPE) as functions of the intrinsic reaction coordinate s over the range −1.0 to 1.0 bohr at the CCSD(T)/B4//BB1K level, where $V_a^G = V_{MEP}$ + ZPE. Although the $V_a{}^G{}_{(s)}$ and V_{MEP} curves are very alike in shape, the locations of the maximum values of the two curves have some differences, which indicate that the variational effects could not be neglected for Channel 1. The variational effect on the rate constant will be tested in the following study (infra). The ZPE curve dropping at near s = 0.25 bohr and shows a noticeable variation with s. This behavior is typical of hydrogen abstraction reaction, and the variation with s is mainly due to a fall in CH_4 stretching corresponding to the normal mode breaking during the reaction, and evolving to the HC_4H stretching mode forming in the product (reactive mode).

The changes in the generalized normal-mode vibrational frequencies at the nonstationary point along the MEPs for Channel 1 are shown in Figure 7. As shown in Figure 7, all frequencies, except the bold black one, do not change significantly during the whole process from reactants to products. The bold black mode changes from 2994 cm^{-1} at s = −1.0 (in reactant zone) to 571 cm^{-1} (s = 0.4) and then to 3435 cm^{-1} at s = 1.0 (in product zone). The closest values of the reactant and product frequencies are 2763 cm^{-1} and 2764 cm^{-1}, corresponding to C−H of CH_4 and C−H of HC_4H stretching, respectively. This mode can therefore be referred to as the "reactive mode" in Channel 1.

The rate constants of the title reaction are calculated over a wide temperature range of 100−3000K by using the conventional transition-state theory (TST), canonical variational transition-state theory (CVT), and CVT with the small-curvature tunneling correction (CVT/SCT) methods. A total of 20 points

Table 1. Calculated Rate Constants along with the Experimental Data for the Title Reaction in the Temperature Range 100−3000 K (cm^3 $molecule^{-1}$ s^{-1}) at the CCSD(T)/aug-cc-pVTZ //BB1K/6-311G(d,p) Level

entry	CCSD(T)/aug-ccpvtz//BB1K//6-311G(d,p)			
T (K)	TST	CVT	CVT/SCT	EXP[27]
100	6.12×10^{-14}	1.74×10^{-14}	2.56×10^{-14}	
110	9.00×10^{-14}	3.07×10^{-14}	4.01×10^{-14}	
125	1.44×10^{-13}	6.13×10^{-14}	7.13×10^{-14}	
143	2.24×10^{-13}	1.17×10^{-13}	1.23×10^{-13}	
167	3.54×10^{-13}	2.27×10^{-13}	2.12×10^{-13}	
200	5.74×10^{-13}	4.40×10^{-13}	3.68×10^{-13}	7.70×10^{-13}
250	9.88×10^{-13}	8.86×10^{-13}	6.88×10^{-13}	
273	1.21×10^{-12}	1.13×10^{-12}	8.41×10^{-13}	
298	1.48×10^{-12}	1.43×10^{-12}	1.01×10^{-12}	
300	1.50×10^{-12}	1.45×10^{-12}	1.03×10^{-12}	2.13×10^{-12}
373	2.44×10^{-12}	2.43×10^{-12}	1.59×10^{-12}	
473	4.13×10^{-12}	4.07×10^{-12}	2.46×10^{-12}	
573	6.38×10^{-12}	5.96×10^{-12}	3.39×10^{-12}	
700	1.02×10^{-11}	8.70×10^{-12}	4.94×10^{-12}	
800	1.40×10^{-11}	1.13×10^{-11}	6.88×10^{-12}	
900	1.87×10^{-11}	1.46×10^{-11}	9.36×10^{-12}	
1000	2.44×10^{-11}	1.85×10^{-11}	1.24×10^{-11}	
1100	3.10×10^{-11}	2.32×10^{-11}	1.60×10^{-11}	
1200	3.88×10^{-11}	2.85×10^{-11}	2.03×10^{-11}	
1300	4.77×10^{-11}	3.46×10^{-11}	2.53×10^{-11}	
1400	5.78×10^{-11}	4.16×10^{-11}	3.11×10^{-11}	
1500	6.93×10^{-11}	4.94×10^{-11}	3.76×10^{-11}	
2000	1.48×10^{-10}	1.03×10^{-10}	8.38×10^{-11}	
3000	4.36×10^{-10}	2.96×10^{-10}	2.58×10^{-10}	

near the transition state (10 on reactants side and 10 on products side) are selected to obtain the potential surface information along the MEP. The calculated TST, CVT, and CVT/SCT rate constants at the CCSD(T)/B4//BB1K level are listed in Table 1 in which available experimental rate constants at temperatures 200 and 300 K are also given.

The CCSD(T)/B4//BB1K/B1 rate constants in the temperature range 100−3000 K and experimental values are plotted as functions of the reciprocal of temperature in Figure 8. In Figure 8, the TST and CVT curves of Channel 1 have some differences at low temperature $T < 250$ K, while the rate constants for TST and CVT are almost the same when $T > 250$ K. This indicates that the variational effect is important in lower temperature region $T <$ 250 K, while it is negligible when $T > 250$ K.

By comparing the CVT/SCT and CVT rate constants, the discrepancy between them when $T > 200$ K implies that the importance of the small-curvature tunneling correction and hence it should be considered in rate constant calculations. The ratio of rate constants between available experimental data[27] and $k_{CVT/SCT}$ (Table 1) are 2.09 and 2.06, indicating an excellent agreement. The normal Arrhenius expression of $k(T) = 8.01 \times 10^{-12} \exp(-615.5 \pm 4.01/T)$ cm^3 $molecule^{-1}$ s^{-1} fits of the CVT/SCT rate constants between 200 and 300 K. Consequently, the calculated activation energy E_a = 1.22 kcal/mol is very close to the experimental value 1.21 kcal/mol.[27]

To facilitate future experimental measurements, the normal (k^2) and three-parameter (k^3) Arrhenius equations fitting of the

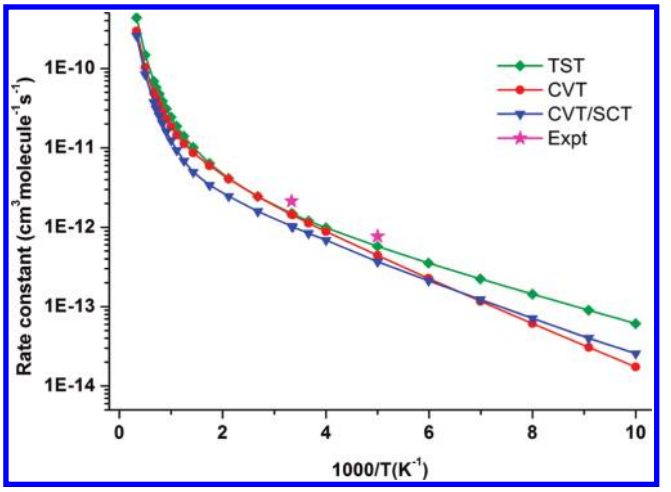

Figure 8. Plot of the TST, CVT, and CVT/SCT rate constants calculated at the CCSD(T)/B4//BB1K/B1 level vs 1000/T between 100 and 3000 K for the title reaction. For clarity, the experimental temperature 200 and 300 K are amplified and given (expt, ref 27).

CVT/SCT rate constants and the activation energies of the title reaction in three temperature ranges from 100 to 3000 K are performed and the expressions are given as follows (in units of cm^3 $molecule^{-1}$ s^{-1}).

$$k^2_{(100-300)} = 6.36 \times 10^{-12} \exp\left(\frac{-558.3}{T}\right)$$

$$\text{Ea} = \frac{1.11 \text{ kcal}}{\text{mol}} [100 \le T \le 300 \text{ K}]$$

$$k^2_{(300-1000)} = 2.56 \times 10^{-11} \exp\left(\frac{-1025.6}{T}\right)$$

$$\text{Ea} = \frac{2.04 \text{ kcal}}{\text{mol}} [300 \le T \le 1000 \text{ K}]$$

$$k^2_{(1000-3000)} = 8.88 \times 10^{-10} \exp\left(\frac{-4494.0}{T}\right)$$

$$\text{Ea} = \frac{8.93 \text{ kcal}}{\text{mol}} [1000 \le T \le 3000 \text{ K}]$$

$$k^3_{(100-300)} = 6.8024 \times 10^{-14} (T)^{0.73152 \exp}\left(\frac{435.3}{T}\right)$$

$$[100 \le T \le 300 \text{ K}]$$

$$k^3_{(300-1000)} = 5.7712 \times 10^{-20} (T)^{2.71723 \exp}\left(\frac{-370.8}{T}\right)$$

$$[300 \le T \le 1000 \text{ K}]$$

$$k^3_{(1000-3000)} = 3.6012 \times 10^{-20} (T)^{2.83019 \exp}\left(\frac{-103.2}{T}\right)$$

$$[1000 \le T \le 3000 \text{ K}]$$

4. CONCLUSION

In this paper, direct ab initio dynamics method was employed to study the title reaction $^{\bullet}C_4H + CH_4$. Two reactive sites of C_4H have been considered and the hydrogen abstraction by C^1 position of the C_4H is the major reaction channel. According to the IRC pathway, the electron transfer behaviors are also analyzed by QRO method in detail, which indicates that it occurs via H-abstraction mechanism conclusively.

The rate constants of Channel 1 are calculated using the TST, CVT, CVT/SCT methods at the CCSD(T)/B4//BB1K/B1 levels of theory over a wide temperature range of 100−3000 K. It is shown that the SCT should be taken into account in the rate constant calculations in $T < 250$ K temperature region, and the variational effect is important in lower temperature range and is, however, negligible in higher temperature region. The CVT/SCT rate constants are in good agreement with available experimental data and the normal Arrhenius expression is $k(T) = 8.01 \times 10^{-12} \exp(-615.5 \pm 4.01/T)$ cm^3 molecule^{-1} s^{-1} between 200 and 300 K. The normal and three-parameter expressions of Arrhenius rate constants are also provided within 100−3000 K. Our theoretical study may be helpful for deeply insight into the reaction dynamics behavior over a wide temperature range where no experimental data is available so far.

■ ASSOCIATED CONTENT

Supporting Information. Cartesian coordinates, harmonic vibrational frequencies (cm^{-1}), and absolute and relative energies for the species discussed are given. Electronic transfer behaviors of Channel 2 in the title reaction are provided. This material is available free of charge via the Internet at http://pubs.acs.org.

■ AUTHOR INFORMATION

Corresponding Author
*E-mail: tcclab@gmail.com.

■ ACKNOWLEDGMENT

This work is supported by the National Natural Science Foundation of China (NSFC No. 21073075), Research Fund for the Doctoral Program of Higher Education of China (RFDP No. 20100061110046), the Special Funding of State Key Laboratory of Theoretical and Computational Chemistry, Jilin University, and Basic Research Fund of Jilin University (No. 421010061439). The authors are thankful for the reviewers' invaluable comments.

■ REFERENCES

(1) Kiefer, J. H.; Sidhu, S. S.; Kern, R. D.; Xie, K.; Chen, H.; Harding, L. B. *Combust. Sci. Technol.* **1992**, *82*, 101–130.
(2) Hausmann, M.; Homann, K. H. *Combust. React. Kinet.* **1991**, *22*, 1–12.
(3) Zhang, H. Y.; McKinnon, J. T. *Combust. Sci. Technol.* **1995**, *107*, 261–300.
(4) Sykes, M. V. *The Future of Solar System Exploration*; Astronomical Society of the Pacific: San Francisco, 2002.
(5) Summers, M. E.; Strobel, D. F. *Astrophys. J.* **1989**, *346*, 495–508.
(6) Kanamori, H.; Hirota, E. *J. Chem. Phys.* **1988**, *89*, 3962–3969.
(7) Heath, J. R., Hammond, G. S., Kuck, V. J., Eds.; *Fullerenes*; American Chemical Society: Washington, DC, 1992.
(8) Minh, Y. C.; van Dishoeck, E. F. *Astrochemistry: From Molecular Clouds to Planetary Systems*; Astronomical Society of the Pacific: San Francisco, 2000.
(9) Millar, T. J.; Farquhar, P. R. A.; Willacy, K. *Astron. Astrophys. Suppl. Ser.* **1997**, *121*, 139–185.
(10) Doty, S. D.; Leung, C. M, L. *Astrophys. J.* **1998**, *502*, 898–908.
(11) Dismuke, K. I.; Graham, W. R. M.; Weltner, W. *J. Mol. Spectrosc.* **1975**, *57*, 127–137.
(12) Gottlieb, C. A.; Gottlieb, E. W.; Thaddeus, P.; Kawamura, H. *Astrophys. J.* **1983**, *275*, 916–921.
(13) Shen, L. N.; Doyle, T. J.; Graham, W. R. M. *J. Chem. Phys.* **1990**, *93*, 1597–1603.
(14) McCarthy, M. C.; Gottlieb, C. A.; Thaddeus, P.; Horn, M.; Botschwina, P. *J. Chem. Phys.* **1995**, *103*, 7820–7827.
(15) Chen, W.; Novick, S. E.; McCarthy, M. C.; Gottlieb, C. A.; Thaddeus, P. *J. Chem. Phys.* **1995**, *103*, 7828–7833.
(16) Hoshina, K.; Kohguchi, H.; Ohshima, Y.; Endo, Y. *J. Chem. Phys.* **1998**, *108*, 3465–3478.
(17) Irvine, W. M.; Hoglund, B.; Friberg, P.; Askne, J.; Ellder, J. *Astrophys. J.* **1981**, *248*, L113–L117.
(18) Bell, M. B.; Sears, T. J.; Matthews, H. E. *Astrophys. J.* **1982**, *255*, L75–L79.
(19) Guelin, M.; Friberg, P.; Mezaoui, A. *Astron. Astrophys. Suppl. Series* **1982**, *109*, 23–31.
(20) Turner, B. E. *Astrophys. J.* **1989**, *347*, L39–L42.
(21) Guélin, M.; Greenan, S.; Thaddeus, P. *ApJ. Lett.* **1978**, *224*, L27–L30.
(22) Friberg, P.; Hjalmarson, A.; Irvine, W. M. *ApJ. Lett.* **1980**, *241*, L99–L103.
(23) Wilson, S.; Green, S. *Astrophys. J. Lett.* **1977**, *212*, L87–L90.
(24) Pauzat, F.; Ellinger, Y.; McLean, A. D. *Astrophys. J. Lett.* **1991**, *369*, L13–L16.
(25) Woon, D. E. *Chem. Phys. Lett.* **1995**, *244*, 45–52.
(26) Zhou, J.; Garand, E.; Eisfeld, W.; Neumark, D. M. *J. Chem. Phys.* **2007**, *127*, 034304–034307.
(27) Berteloite, C.; Le Picard, S. D.; Balucani, N.; Canosa, A.; Sims, I. R. *Phys. Chem. Chem. Phys.* **2010**, *12*, 3666–3676.
(28) Zhao, Y.; Lynch, B. J.; Truhlar, D. G. *J. Phys. Chem. A.* **2004**, *108*, 2715–2719.
(29) Scuseria, G. E.; Schaefer, H. F. *J. Chem. Phys.* **1989**, *90*, 3700–3703.
(30) Pople, J. A.; Gordon, M. H.; Raghavachari, K. *J. Chem. Phys.* **1989**, *87*, 5968–5975.
(31) Frisch, M. J.; Trucks, G. W.; Schlegel, H. B.; Scuseria, G. E.; Robb, M. A.; Cheeseman, J. R.; Montgomery, J. A., Jr.; Vreven, T.; Kudin, K. N.; Burant, J. C., Millam, J. M.; Iyengar, S. S.; Tomasi, J.; Barone, V.; Mennucci, B.; Cossi, M.; Scalmani, G.; Rega, N.; Petersson, G. A.; Nakatsuji, H.; Hada, M.; Ehara, M.; Toyota, K.; Fukuda, R.; Hasegawa, J.; Ishida, M.; Nakajima, T.; Honda, Y.; Kitao, O.; Nakai, H.; Klene, M.; Li, X.; Knox, J. E.; Hratchian, H. P.; Cross, J. B.; Bakken, V.; Adamo, C.; Jaramillo, J.; Gomperts, R.; Stratmann, R. E.; Yazyev, O.; Austin, A. J.; Cammi, R.; Pomelli, C.; Ochterski, J. W.; Ayala, P. Y.; Morokuma, K.; Voth, G. A.; Salvador, P.; Dannenberg, J. J.; Zakrzewski, V. G.; Dapprich, S.; Daniels, A. D.; Strain, M. C.; Farkas, O.; Malick, D. K.; Rabuck, A. D.; Raghavachari, K.; Foresman, J. B.; Ortiz, J. V.; Cui, Q.; Baboul, A. G.; Clifford, S.; Cioslowski, J.; Stefanov, B. B.; Liu, G.; Liashenko, A.; Piskorz, P.; Komaromi, I.; Martin, R. L.; Fox, D. J.; Keith, T.; Al-Laham, M. A.; Peng, C. Y.; Nanayakkara, A.; Challacombe, M.; Gill, P. M. W.; Johnson, B.; Chen, W.; Wong, M. W.; Gonzalez, C.; Pople, J. A. *Gaussian 03*, Revision D.02, Gaussian, Inc.: Wallingford, CT, 2004.
(32) Corchado, J. C.; Chuang, Y.-Y.; Fast, P. L.; Hu, W.-P.; Liu, Y.-P.; Lynch, G. C.; Nguyen, K. A.; Jackels, C. F.; Ramos, A. F.; Ellingson, B. A.; Lynch, B. J.; Zheng, J.; Melissas, V. S.; Villà, J.; Rossi, I.; Coitino, E. L.; P., Jingzhi; Albu, T. V. *Department of Chemistry and Supercomputing Institute*; University of Minnesota: Minneapolis, MN, 2007, Version 9.7.
(33) Liu, Y. P.; Lynch, G. C.; Truong, T. N.; Lu, D. H.; Truhlar, D. G.; Garrett, B. C. *J. Am. Chem. Soc.* **1993**, *115*, 2408–2415.

(34) Garrett, B. C.; Truhlar, D. G. *J. Chem. Phys.* **1979**, *70*, 1593–1598.
(35) Garrett, B. C.; Truhlar, D. G. *J. Am. Chem. Soc.* **1979**, *101*, 4534–4548.
(36) Neese, F. *J. Am. Chem. Soc.* **2006**, *128*, 10213–10222.
(37) Neese, F. *ORCA—an ab initio, density functional and semiempirical program package*, Version 2.8; Bonn University: Germany, 2010.
(38) Pettersen, E. F.; Goddard, T. D.; Huang, C. C.; Couch, G. S.; Greenblatt, D. M.; Meng, E. C.; Ferrin, T. E. *J. Comput. Chem.* **2004**, *25*, 1605–1612.
(39) Stephens, J. W.; Yan, Wen-Bin; Richnow, M. L.; Solka, H.; Curl, R. F. *J. Mol. Struct.* **1988**, *190*, 41–60.
(40) Bogey, M.; Demuynck, C.; Destombes, J. L. *Mol. Phys.* **1989**, *66*, 955–960.
(41) Hirota, E. *J. Mol. Spectrosc.* **1979**, *77*, 213–221.
(42) Sverdlov, L. M.; Kovner, M. A.; Krainov, E. P. *Vibrational spectra of polyatomic molecules*; Wiley: New York. 1974.
(43) Herzberg, G.; *Electronic spectra and electronic structure of polyatomic molecules*; Van Nostrand: New York, 1966.
(44) Hellwege, K. In *Group II: Atomic and Molecular Physics Vol. 7: Structure Data of Free Polyatomic Molecules*Landolt-Bornstein, A. H., Ed.; Springer-Verlag: Berlin, 1976.